Check for updates

Recycling of polystyrene waste to mono-aromatic hydrocarbons *via* intermittent thermal scission†

Zhuohan Lin, [iD] [a] Jiaxin Li,[a] Wang Xu,[a] Qiaohui Ruan,[a] Jiakang Hu,[a] Peiqing Yuan[b] and Yan Li [iD] *[a]

Polystyrene (PS) is a widely used plastic that contributes significantly to plastic waste. Chemical recycling of PS into valuable industrial mono-aromatic hydrocarbons (MAHs) offers a promising approach for mitigating the environmental impact of PS waste while simultaneously valorizing it. However, current methods typically achieve MAH yields of less than 75%, with limited potential for significant improvement. Here, we propose a novel cyclic depolymerization and repolymerization strategy to precisely control PS pyrolysis without catalysts. This method alternates depolymerization at around 400 °C with repolymerization at around 300 °C in a semi-batch system, achieving an unprecedented MAH yield (MAH selectivity up to 95% with liquid yields exceeding 90 wt%). Repolymerization forms cross-linked structures, effectively suppressing oligomer formation and converting low-reactivity oligomers into more reactive polymer segments, which is crucial for achieving extraordinarily high MAH yields. This "intermittent" scission strategy is broadly applicable to diverse PS waste streams, highlighting its potential for sustainable waste management.

Green foundation

1. This work presents an innovative, catalyst-free approach for polystyrene (PS) upcycling, effectively eliminating the need for harmful substances. This method provides a cleaner, safer, and more sustainable alternative to conventional chemical recycling processes.

2. We have successfully employed an "intermittent" thermal scission strategy to convert PS waste into mono-aromatic hydrocarbons (MAHs), achieving exceptional selectivity up to 95% and liquid yields exceeding 90 wt%. These results notably surpass conventional PS recycling methods, which typically achieve MAH yields of less than 75%. Additionally, our process operates at lower temperatures compared to traditional methods, significantly enhancing energy efficiency.

3. Future research could enhance sustainability by applying polymer structure-controlled kinetics to complex and mixed plastic wastes. Integrating selective catalytic processes with our thermal approach may enable milder conditions, increasing versatility and environmental benefits.

Introduction

Over the past half-century, plastics have driven technological progress and brought convenience to daily life; however, increasing demand, short lifecycles and non-biodegradability have turned their management and recycling into urgent global challenges.[1–3] Polystyrene (PS), one of the most widely used plastics globally, is commonly employed in food packaging, disposable tableware and construction materials. Although PS, like most thermoplastics, can be mechanically recycled, its performance degrades over successive cycles, limiting its range of applications.[4] Chemical recycling,[5–10] which converts PS into valuable chemicals, particularly widely-used industrial monocyclic aromatic hydrocarbons (MAHs) such as styrene, toluene, ethylbenzene and α-methyl styrene, has emerged as a promising alternative.[11]

The primary chemical recycling methods for PS involve catalytic and non-catalytic pyrolysis, typically conducted at temperatures between 380 °C and 600 °C, with MAH yields ranging from 50 wt% to 75 wt% (Fig. 1a).[12–14] Catalytic pyrolysis often employs solid acid catalysts, including zeolites,[15] metal oxides[16] or supported metal catalysts.[17] However, during catalytic pyrolysis, benzene rings may undergo ring-opening, resulting in gas formation. The high molecular weight and viscosity of PS also limit diffusion, making the phenyl side

[a]Key Laboratory for Advanced Materials, Shanghai Key Laboratory of Functional Materials Chemistry, School of Chemistry and Molecular Engineering, East China University of Science and Technology, Shanghai 200237, China. E-mail: yli@ecust.edu.cn
[b]State Key Laboratory of Chemical Engineering, School of Chemical Engineering, East China University of Science and Technology, Shanghai 200237, China
†Electronic supplementary information (ESI) available. See DOI: https://doi.org/10.1039/d5gc01563d
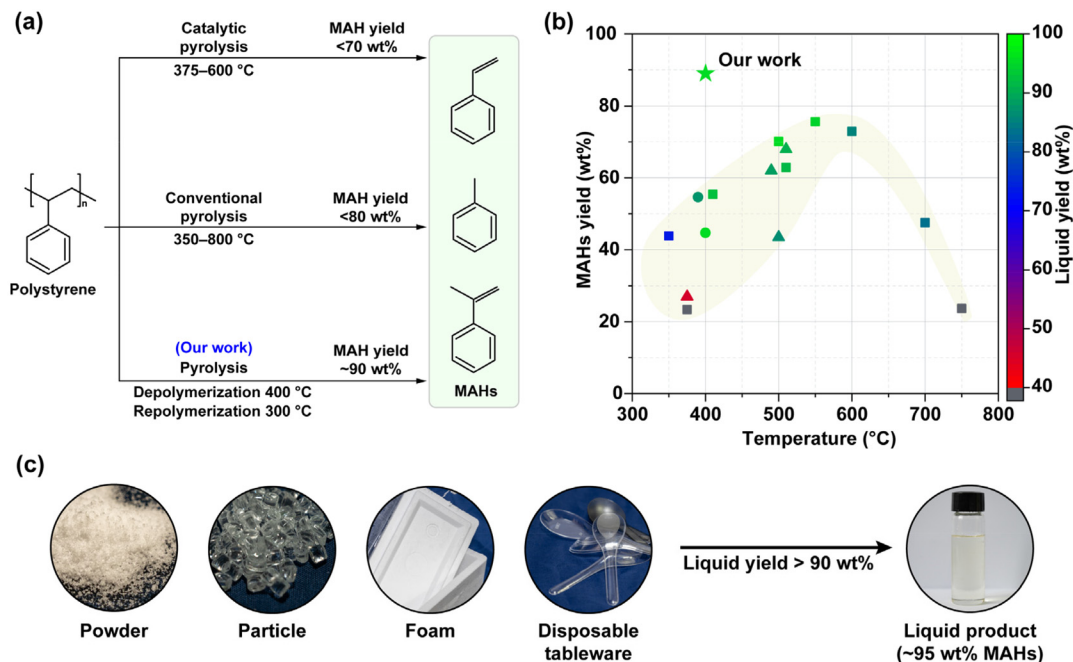
Fig. 1 (a) Schematic illustration of catalytic pyrolysis, pyrolysis, and our method for recycling of PS to obtain MAHs. (b) Statistical plots of liquid yields at different pyrolysis temperatures as well as selectivity of MAHs in the liquid from typical studies[12–15,17,19,20,22,23,25–28] and data from our work (liquid yield is indicated by color mapping; squares indicate pyrolysis, circles indicate co-pyrolysis, and triangles indicate catalytic pyrolysis). The light-yellow belt shows the variation of MAH yields with temperature based on the results in the literature. (c) Scheme of conversion of different types of PSs into MAHs by cyclic Dp–Rp pyrolysis.

chains prone to aromatization and coke formation.[18] The formation of gas and coke together restricts improvements in liquid yield and MAH yields. Moreover, coke formation, along with additives and contaminants present in waste PS, can reduce catalyst activity and compromise long-term stability.[19] Therefore, while catalytic pyrolysis holds great potential for PS recycling, it requires special effort in designing robust catalysts and precise control over the reaction process.

The non-catalytic pyrolysis of PS is typically initiated by random scission of the backbone, followed by the main reaction, β-scission, to produce styrene monomers. Although the C–C bonds in the main chain can break at approximately 325 °C, diffusion limitations caused by high viscosity promote radical coupling, which reduces the initiation efficiency of pyrolysis and hinders effective depolymerization.[20,21] For instance, Serrano et al. reported a liquid yield of only 36 wt% after 30 min at 375 °C in a batch reactor.[15] Artetxe et al. showed that rapid pyrolysis of PS in a conical spouted bed reactor at 550 °C could increase MAH yield to 75 wt%.[22] Although MAH selectivity can exceed 70% at temperatures above 500 °C, the kinetic characteristics of conventional constant-temperature pyrolysis inevitably lead to the formation of undesirable byproducts, such as dimers and trimers, through intramolecular hydrogen transfers.[23,24] MAH selectivity was suboptimal at pyrolysis temperatures below 500 °C or above 600 °C (Fig. 1b). Therefore, further improving MAH selectivity remains a significant challenge using conventional pyrolysis methods, regardless of catalyst use.

Herein, we present a novel "intermittent" thermal scission strategy based on a cyclic depolymerization and repolymerization (Dp–Rp) process, which enables precise control over the pyrolysis reaction network and achieves extraordinarily high yields in the conversion of PS to MAHs. Thermodynamically, PS depolymerizes at approximately 400 °C to produce MAHs and subsequently repolymerizes at around 300 °C, forming a cross-linked polymer structure. The repolymerization step effectively converts low-reactivity oligomers into more reactive polymer segments. Importantly, the cross-linked polymer structure formed during repolymerization restricts intramolecular hydrogen transfer reactions, thereby suppressing oligomer formation. By implementing dynamic temperature regulation, we achieved a liquid yield exceeding 90 wt% and an MAH selectivity as high as 95 wt% in a semi-batch reactor (Fig. S1†). Remarkably, this method is applicable to various types of PS waste, consistently delivering similarly high MAH yields (Fig. 1c).

Experimental section

Materials

Polystyrene (PS) powders with a weight average molecular weight of roughly 140 000 g mol^{-1} were obtained from China Petrochemical Corporation. General-purpose PS pellets of similar molecular weight were supplied by Adamas-beta, and expandable PS beads (~90 000 g mol^{-1}) came from BASF. Used

PS tableware was purchased locally and employed as a representative post-consumer waste. Analytical-grade dichloromethane, deuterated chloroform containing 0.03% tetramethylsilane, toluene, *n*-heptane, styrene, ethylbenzene, cumene and α-methyl-styrene (all ≥99%) were used without further purification.

Reactor and pyrolysis procedures

All experiments were carried out in a 250 mL stainless-steel autoclave fitted with a mechanical stirrer, an external resistance heating (800 W) system and a water-cooled condenser (Fig. S1†). The reactor was purged three times with high-purity nitrogen and then maintained at 0.1 MPa N_2 for each run.

For batch pyrolysis, 30 g of PS powder was heated from room temperature to 400 °C at 10 °C min^{-1} under stirring at 150 rpm. The temperature was held for 5, 10 or 15 min, after which the heater was removed and the vessel was quenched in cold water to stop the reaction.

Semi-batch operation followed the same heating profile, but the condenser valve remained open throughout. Volatile products condensed continuously until the liquid flow ceased, typically after about 30 min.

Dp–Rp experiments were performed under semi-batch conditions. 30 g of PS (or 10 g for foam and waste samples) was processed in successive cycles between a high temperature T_H of 390–410 °C and a low temperature T_L of 300 °C. The reactor was heated to T_H, removed from the furnace and allowed to cool naturally to T_L (∼−10 °C min^{-1}), then reheated. Liquid products were collected at each high-temperature stage. One to four cycles were carried out, and every experiment was repeated at least three times to ensure reproducibility.

Product analysis

Condensate mass was recorded after each cycle and the overall liquid yield was calculated as the ratio of total condensate to initial feed mass. Chemical compositions were identified by GC-MS (Shimadzu GC-2010, DB-5 ms capillary column, NIST-14 library, match probability >95%). Quantitative analyses were performed employing GC-FID (Agilent 6890 N, HP-5 column) with *n*-heptane as the internal standard. Response factors were determined from calibration curves and used to calculate mono-aromatic hydrocarbon selectivities. Spectroscopic characterisation included FT-IR (KBr disks, 4000–400 cm^{-1}, 24 scans) and ^{1}H/^{13}C NMR (400/600 MHz, CDCl$_3$). Elemental analysis was conducted using an Elementar vario EL cube analyzer, with each sample measured in duplicate.

Residue characterisation

Melt residues sampled rapidly at 300 °C and 400 °C were analysed immediately by electron paramagnetic resonance (Bruker EMXnano) to quantify persistent radicals. ^{13}C NMR and DEPT-135 spectra (600 MHz) provided structural information, while molecular-weight distributions were measured by GPC in THF (Agilent 1260) calibrated with PS standards.

Computational methods

Representative pyrolysis intermediates were optimised at the B3LYP/6-311+G(2d,p) level with chloroform as the implicit solvent using Gaussian 09. Scaled ^{13}C chemical shifts[29] were obtained from the optimised geometries using Multiwfn[30] and compared with experimental data.

Results & discussion

The pyrolysis of PS has been extensively studied, primarily following the reaction mechanism proposed by Broadbelt[31,32] and Faravelli,[24] as depicted in Fig. 2. Initially, the PS main chain undergoes random scission, generating equal amounts of primary carbon radicals (#1) and secondary carbon radicals (#2). These radicals can form styrene monomers *via* β-scission, which is the primary pathway for obtaining styrene. During pyrolysis, radicals #1 and radicals #2 can also undergo intermolecular hydrogen transfer reactions with the PS main chain, generating tertiary carbon radicals (#3). Radicals #3 produce PS segments with terminal double bonds (P-OT) and radicals #2 *via* β-scission. Notably, radicals #2 can undergo intramolecular 1,3- and 1,5-hydrogen transfers, forming more stable tertiary carbon radicals 3#3 and 5#3. These tertiary carbon radicals can then undergo β-scission *via* two different pathways: when the cleavage site is distant from the chain end, dimers, trimers and new radicals #2 are produced; when the cleavage site is near the chain end, P-OT, benzyl radicals (#Tol) and 1,3-diphenylpropane radicals (DPP) are produced. The terminal P-OT can undergo homolysis to generate α-methyl styrene radicals (#αMS) and radicals #2. Small radicals such as #Tol, #DPP, and #αMS can be converted to toluene, 1,3-diphenylpropane and α-methyl styrene, respectively, through intermolecular hydrogen transfer reactions. Consequently, even in the absence of diffusion limitations in the reaction system, the liquid products of PS pyrolysis still include dimers, trimers, and 1,3-diphenylpropane, in addition to MAHs such as styrene, toluene, and α-methylstyrene.

To verify the impact of intramolecular hydrogen transfer on MAH selectivity, PS pyrolysis was conducted at a constant temperature of 400 °C using a semi-batch reactor, which facilitated the timely escape of generated MAHs and effectively suppressed secondary reactions (see ESI for details†). The total liquid yield reached 94.5 wt%, with styrene as the main component (the qualitative results of products are presented in Fig. S2†). The MAH yield reached 70.7 wt%, but the liquid products still contained approximately 25 wt% of dimers, trimers, and higher molecular weight oligomers.

According to the PS pyrolysis mechanism and experimental results, achieving high-selectivity conversion of PS to MAHs requires suppressing 1,3- and 1,5-hydrogen transfer of radicals #2 to minimize the formation of undesired byproducts such as dimers and trimers. Additionally, inactive oligomers formed during the reaction should be converted back into active polymer segments that can undergo further cracking more efficiently.
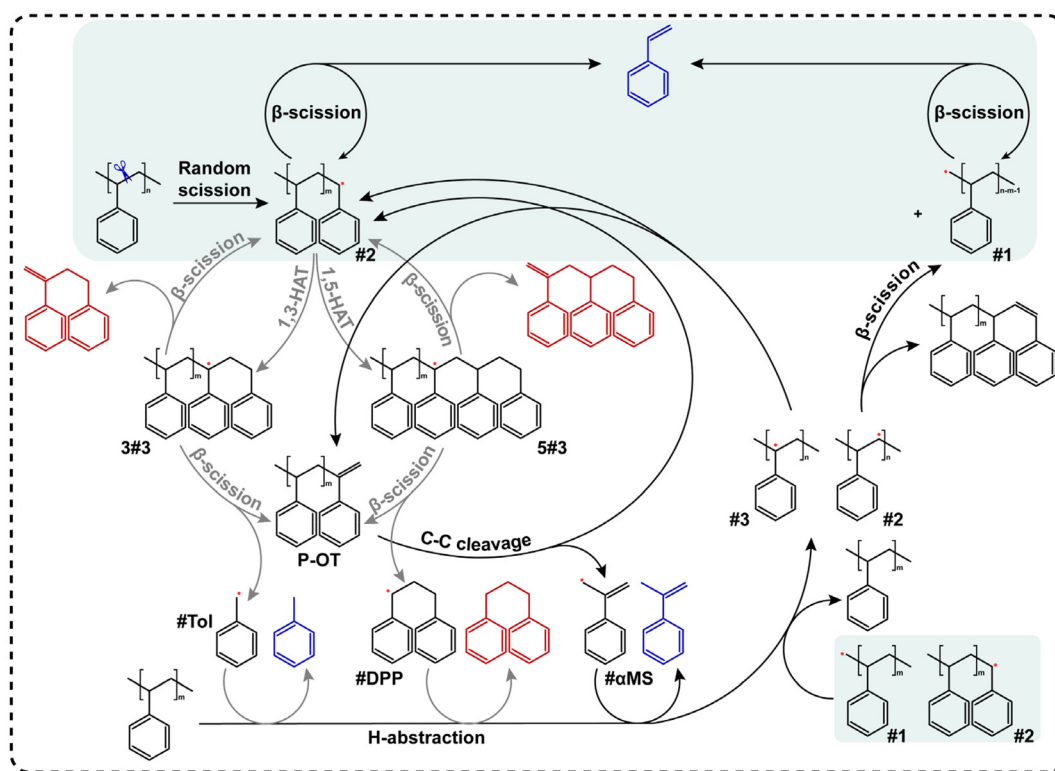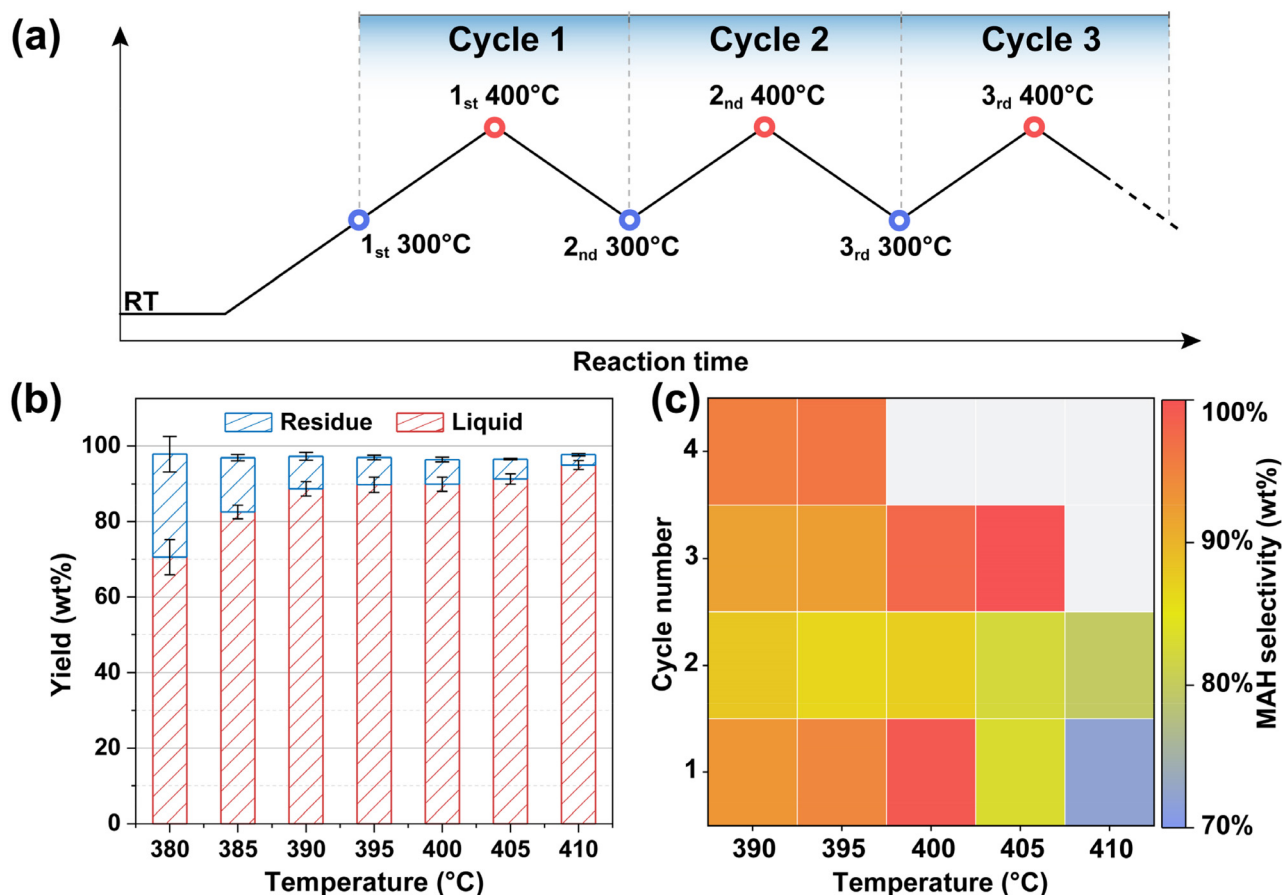
Fig. 2 Schematic illustration of the main reaction process of PS pyrolysis.[24,29,30]

To suppress secondary reactions and intramolecular hydrogen transfers in the conventional pyrolysis and enhance MAH yield, a unique pyrolysis method based on a cyclic Dp–Rp process was carried out using a semi-batch reactor. PS pyrolysis follows a radical reaction mechanism, where the random scission of the polymer backbone and the repolymerization of the polymer segments can be viewed as forward and reverse reactions, respectively. The depolymerization is an endothermic, entropy-increasing process with a high activation energy, typically requiring elevated temperatures to proceed effectively, while the repolymerization is an exothermic, entropy-decreasing process with a low activation energy, allowing it to occur rapidly even at low temperatures. To optimize this process, we selected two distinct reaction temperature ranges: a higher temperature (T_H, 380–410 °C) for polymerization of PS, which primarily produces MAHs, and a lower temperature (T_L, 300 °C) for repolymerization. During repolymerization, a cross-linked polymer network is expected to form, which should effectively reincorporate the generated oligomers into the polymer matrix while hindering intramolecular hydrogen transfer.

Typically, a certain amount of PS powder was added to the reactor (Fig. S1†). After purging the system with nitrogen, the reactor was heated at a set rate to the target T_H (380–410 °C), passing through T_L (260–340 °C). Upon reaching T_H, the system temperature was immediately lowered to T_L at a set cooling rate, completing the first T_L–T_H–T_L cycle (Fig. 3a). Subsequently, the temperature was increased again to initiate the next T_L–T_H–T_L cycle. Once the system temperature exceeds 350 °C, liquid products typically begin to flow out and are collected during each cycle. The reaction is considered complete when no liquid product is observed during a cycle (typical temperature curves are presented in Fig. S3†).

Lowering the system temperature to T_L is expected to promote cross-linking of residual PS, enabling structural rearrangement prior to further thermal cracking. To assess the influence of T_L on product distribution, experiments were conducted at T_L values of 340 °C, 300 °C, and 260 °C at a fixed T_H of 400 °C (yields of liquid products and residues are shown in Fig. 3b and Fig. S4†). As shown in Table S1,† T_L = 340 °C gave the highest liquid yield during the second cycle but the lowest overall MAH selectivity, indicating that significant PS cracking still occurred at this temperature. At T_L = 340 °C, the molecular weight of the residual polymer decreased with cycling, and only weak ^{13}C NMR signals were observed (Fig. S5†), consistent with dominant cracking and limited repolymerization. In contrast, T_L = 300 °C led to a pronounced increase in residual molecular weight and more complex ^{13}C NMR profiles, indicating enhanced cross-linking. A further decrease to 260 °C produced no additional molecular weight increase. These results demonstrate that while T_L had limited impact on overall liquid yield—primarily dictated by T_H—it played a critical role in tuning MAH selectivity by regulating the extent of cross-linking. Accordingly, T_L = 300 °C was selected for subsequent experiments to balance energy input and structural evolution.

Fig. 3 (a) Schematic illustration of the typical cyclic Dp–Rp pyrolysis process at a T_H of 400 °C. (b) Histogram of yields of liquid products and residues obtained from the pyrolysis of PS at different T_H. (c) Heatmap of MAH selectivity in liquid products of different cycles obtained by the pyrolysis of PS at different T_H.

The relationship between system temperature and reaction time under different heating rates (corresponding to different heating powers) is shown in Fig. S3.† At 100% of the rated power of the furnace, the temperature increased from T_L to T_H within 12 min, maintaining MAH selectivity above 85% in the second and third cycles. When the heating power was reduced to 70%, the heating time extended significantly to 25 min, causing the first cycle to contribute over 50% of the total liquid yield and diminishing the effectiveness of the Dp–Rp strategy in later cycles (Table S1†). Cooling methods, including air and water bath cooling, were also evaluated. As shown in Table S1,† the cooling rate had negligible influence on either the total liquid yield or MAH selectivity. Therefore, 100% power heating and air cooling were employed in all systematic experiments to ensure consistent thermal cycling between T_L and T_H.

As shown in Fig. 3b, the value of T_H significantly impacts the reaction rate of pyrolysis, influencing both the number of cycles required to reach the reaction endpoint and the resulting liquid yield. When T_H is set to 380–385 °C, 390–395 °C, 400–405 °C and 410 °C, the required number of cycles is 5, 4, 3, and 2, respectively. As T_H increases, the liquid yield gradu-

ally rises from 70.6 wt% at 380 °C to 96.2 wt% at 410 °C. GC-MS analysis revealed that the types of compounds in the liquid products obtained across different cycles at various T_H were consistent, differing only in their concentrations. All liquid samples mainly contained styrene, toluene and α-methyl styrene as major MAHs, along with minor amounts of dimers 1,3-diphenyl-1-butene and 1,3-diphenylpropane. Almost no trimers were detected in all liquid products.

After the reaction, approximately 5–10 wt% of high-boiling residues remain at the bottom of the reactor. These residues are nicely soluble in various organic solvents such as dichloromethane, toluene and tetrahydrofuran, and no insoluble residues such as coke were observed. The relatively low reaction temperature in this study (below 410 °C) results in negligible gas generation. Under typical Dp–Rp conditions ($T_H = 400$ °C, $T_L = 300$ °C), carbon and hydrogen recoveries reached 96% (Table S2†). Given the minimal gas formation, hydrogen loss to the gas phase is considered negligible.

Taking the liquid products obtained at a T_H of 400 °C as an example, the Fourier transform infrared spectroscopy data (Fig. S6†) reveal that samples from all three cycles exhibit similar absorption characteristics. As the number of cycles

increases, the out-of-plane bending vibration peak of the $R_2C=CH_2$ group, which corresponds to $=C–H$ at 890 cm^{-1}, becomes more pronounced. In the ^1H nuclear magnetic resonance spectra (Fig. S7†), signals for the methyl hydrogen in toluene and α-methyl styrene appear at chemical shifts (δ) of 2.14 ppm and 2.33 ppm, respectively, with their intensities increasing as the number of cycles progresses. The results suggest as the cyclic reaction progresses, the concentrations of toluene and α-methylstyrene in the liquid products gradually increase.

Quantitative analysis of MAHs in the liquid products was conducted using gas chromatography-flame ionization detection (GC-FID), with representative chromatograms displayed in Fig. S8† and MAH selectivity shown in Fig. 3c. For a given T_H, the styrene concentration gradually declined with successive cycles, while toluene and α-methyl styrene concentrations increased. When T_H was in the range of 380–405 °C, MAH selectivity in all liquid samples exceeded 80%, with styrene as the main component in each cycle. Notably, the total MAH selectivity reached 95 wt% when T_H was set to 400 °C.

Based on the designed cyclic pyrolysis method, PS undergoes pyrolysis at the higher temperature of around T_H and repolymerization at a lower temperature of around T_L. Taking the cyclic pyrolysis process with a set T_H of 400 °C as an example, reactor residues were sampled at both T_H and T_L for

characterization using gel permeation chromatography (GPC) and electron paramagnetic resonance (EPR) (Fig. S9 and Table S3†). During the first cycle, as the system was heated to 300 °C, the weight-average molecular weight (M_w) of the residues decreased from approximately 140 000 to 96 828 (Fig. 4a). This suggests that the PS backbone did not undergo large-scale random scission, which aligns with the EPR analysis (Fig. S10†), showing no significant radical signal. When the temperature was increased to 400 °C, the M_w sharply decreased to 12 555, accompanied by a pronounced radical signal, confirming accelerated cracking. Lowering the temperature back to 300 °C to complete the first T_L–T_H–T_L cycle resulted in a slight increase in M_w compared to that at 400 °C, suggesting repolymerization of radical-containing PS segments. In the second cycle, heating to 400 °C caused a significant M_w decrease and a rapid increase in radical concentration, confirming effective cracking. Notably, upon cooling back to 300 °C, M_w increased significantly, with the GPC profile displaying two distinct peaks. As the radical concentration increased, the cross-linking reaction proceeded more rapidly during the second cycle, causing a notable rise in molecular weight (Table S3†). By the end of the second cycle, M_w was markedly higher than at the end of the first cycle, indicating a shift in the repolymerization pattern.
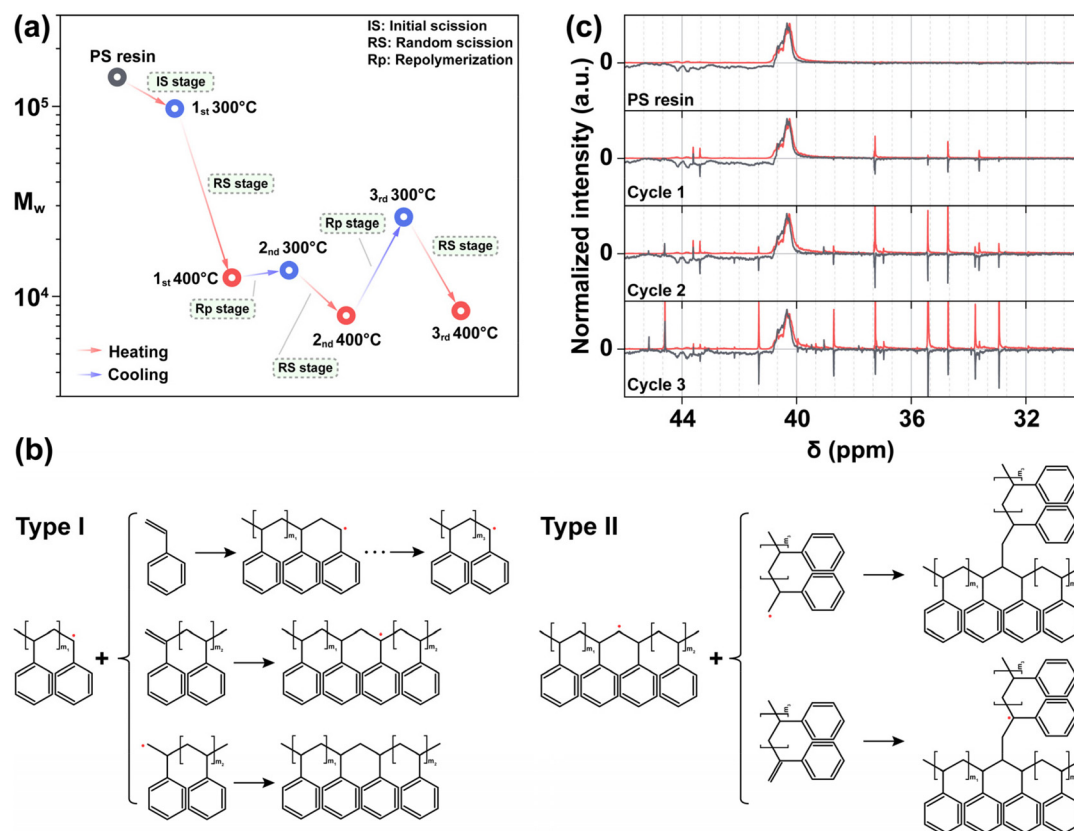
Fig. 4 (a) Plot of the molecular weight of unreacted PS in the autoclave at different stages of cyclic Dp–Rp pyrolysis. (b) Schematic diagram of the repolymerization process at a T_L of 300 °C. (c) ^{13}C NMR spectra (red line) and DEPT135 spectra (gray line) of PS resin and residues in an autoclave obtained by sampling at a T_L of 300 °C.

During the temperature reduction to T_L, two possible repolymerization patterns may occur: linear growth and branching. Based on reported hydrocarbon radical reaction mechanisms,[31] possible reactions for linear growth include: radical addition of styrene and oligomers (P-OT) to primary carbon radicals #1 and coupling of primary carbon radicals #1 (Fig. 4c). The branching process involves the addition or coupling of olefin groups or radical ends from the above substances with secondary carbon radicals #2 and tertiary carbon radicals #3 (Fig. 4c). Linear chain growth increases the M_w while preserving a linear structure, whereas frequent branching leads to the formation of a cross-linked network structure.

To investigate the repolymerization progress, the ^{13}C NMR spectra and distortionless enhancement by polarization transfer (DEPT135) spectra of the residues at temperature T_L are shown in Fig. 4b, alongside data for the PS feedstock for comparison. The ^{13}C NMR spectrum of the PS feedstock displays characteristic peaks at δ of 44 ppm and 40 ppm, corresponding to secondary and tertiary carbons, respectively. In the DEPT135 spectrum, secondary carbons appear as negative peaks, and tertiary carbons as positive peaks. During cyclic pyrolysis, all 300 °C samples exhibited multiple new peaks in the 44–32 ppm range, with intensities increasing over successive cycles. Density functional theory (DFT) calculations (Fig. S11†) indicate that cross-linking at primary or tertiary carbon sites shifts their chemical resonance to lower fields, correlating with the peak near δ of 44 ppm in Fig. 4b. The results confirm the formation of a cross-linked structure during repolymerization. The degree of branching increases notably with the number of cycles, as evidenced by the significant rise in M_w of the residue (Fig. 4a). Additionally, the increasing concentrations of toluene and α-methyl styrene, primarily deriving from reactions at chain ends, further indicate the proliferation of branches during repolymerization.

The formation of dimers and trimers involves intramolecular 1,3- and 1,5-hydrogen transfer of secondary carbon radicals (#2), requiring specific four- or six-membered cyclic transition states. During the cyclic Dp–Rp pyrolysis, the cross-linked network formed by repolymerization effectively suppresses the formation of these circular transition states, resulting in minimal dimer content and negligible trimer formation. Additionally, the relatively low T_H (around 400 °C) limits oligomer escape, keeping them in the liquid phase, where they are reconstituted into polymer segments during repolymerization. Consequently, this repolymerization process not only suppresses oligomer formation but also converts low-activity oligomers into high-activity polymer segments, ensuring exceptionally high MAH selectivity.

To validate the versatility of cyclic Dp–Rp pyrolysis, we pyrolyzed PS resins with different morphologies (granules and foam) and post-consumer PS plastics (disposable tableware and foamed packaging, Fig. 1c). The MAH selectivity in the liquid products consistently exceeds 90 wt% across all feedstocks (Table S4†). These results indicate that PS morphology, along with additives and impurities, has almost no significant impact on the liquid distribution achieved by this proposed pyrolysis method.

Conclusions

In summary, we dynamically couple Dp–Rp processes to control PS cracking, achieving extraordinarily high liquid yields (>93 wt%) and MAH selectivity (up to 95 wt%) under relatively mild conditions (ambient pressures, 300–400 °C). The reaction process was monitored using GPC, EPR and NMR, revealing distinct reaction mechanisms at different temperature stages (around 400 °C for T_H and 300 °C for T_L) and highlighting the critical role of effectively combining depolymerization and repolymerization. In the high-temperature stage, the polymer efficiently cracks to produce styrene-dominated MAHs. In the low-temperature stage, repolymerization occurs, forming cross-linked polymer structures. The repolymerization process not only converts low-activity oligomers into cracking-active polymer segments but also generates a cross-linked network that limits the formation of cyclic transition states necessary for intramolecular hydrogen transfer, thereby suppressing dimer and trimer formation. Our results from PS resins and waste PS plastics demonstrate its potential for diverse feedstocks. This advancement, which achieves precise control over the reaction pathway through dynamic temperature regulation, provides a novel and efficient model for highly selective polymer cracking.

Author contributions

Z. L. performed all experiments and wrote the manuscript. J. L., W. X., Q. R. and J. H. provided some help with experimental improvement and writing. P. Y. and Y. L. provided constructive guidance on the overall design of the experiments. All the authors discussed the results and commented on the paper.

Conflicts of interest

The authors declare no competing interests.

Data availability

Some relevant data are within the manuscript. The data supporting this article have been included as part of the ESI.†

Acknowledgements

References

1 B. M. Weckhuysen, *Science*, 2020, **370**, 400–401.

2 L. T. J. Korley, T. H. Epps, B. A. Helms and A. J. Ryan, *Science*, 2021, **373**, 66–69.

3 M. MacLeod, H. P. H. Arp, M. B. Tekman and A. Jahnke, *Science*, 2021, **373**, 61–65.

4 I. Vollmer, M. J. F. Jenks, M. C. P. Roelands, R. J. White, T. van Harmelen, P. de Wild, G. P. van der Laan, F. Meirer, J. T. F. Keurentjes and B. M. Weckhuysen, *Angew. Chem., Int. Ed.*, 2020, **59**, 15402–15423.

5 F. Zhang, M. Zeng, R. D. Yappert, J. Sun, Y.-H. Lee, A. M. LaPointe, B. Peters, M. M. Abu-Omar and S. L. Scott, *Science*, 2020, **370**, 437–441.

6 W. Zhang, S. Kim, L. Wahl, R. Khare, L. Hale, J. Hu, D. M. Camaioni, O. Y. Gutiérrez, Y. Liu and J. A. Lercher, *Science*, 2023, **379**, 807–811.

7 Z. Xu, N. E. Munyaneza, Q. Zhang, M. Sun, C. Posada, P. Venturo, N. A. Rorrer, J. Miscall, B. G. Sumpter and G. Liu, *Science*, 2023, **381**, 666–671.

8 H. Li, J. Wu, Z. Jiang, J. Ma, V. M. Zavala, C. R. Landis, M. Mavrikakis and G. W. Huber, *Science*, 2023, **381**, 660–666.

9 R. J. Conk, S. Hanna, J. X. Shi, J. Yang, N. R. Ciccia, L. Qi, B. J. Bloomer, S. Heuvel, T. Wills, J. Su, A. T. Bell and J. F. Hartwig, *Science*, 2022, **377**, 1561–1566.

10 Q. Ma, Y. Gao, B. Sun, J. Du, H. Zhang and D. Ma, *Nat. Commun.*, 2024, **15**, 8243.

11 M. Razzaq, M. Zeeshan, S. Qaisar, H. Iftikhar and B. Muneer, *Fuel*, 2019, **257**, 116119.

12 P. L. Beltrame, L. Bergamasco, P. Carniti, A. Castelli, F. Bertini and G. Audisio, *J. Anal. Appl. Pyrolysis*, 1997, **40–1**, 451–461.

13 A. Karaduman, E. H. Simsek, B. Çiçek and A. Y. Bilgesü, *J. Anal. Appl. Pyrolysis*, 2002, **62**, 273–280.

14 A. Karaduman, E. H. Simsek, B. Çiçek and A. Y. Bilgesü, *J. Anal. Appl. Pyrolysis*, 2001, **60**, 179–186.

15 D. P. Serrano, J. Aguado and J. M. Escola, *Appl. Catal., B*, 2000, **25**, 181–189.

16 J. Nisar, G. Ali, A. Shah, M. N. Ashiq, Z. H. Farooqi, A. Sharif, E. Ahmed, M. Iqbal, S. T. H. Sherazi and M. R. Shah, *Waste Manage. Res.*, 2020, **38**, 1269–1277.

17 Z. Zhang, Q. Cheng, C. Shan, Y. Jiang, G. Kong, G. Zhang, S. T. Gopakumar, S. Shi, X. Zhang, L. Han and J. Anal, *Appl. Pyrolysis*, 2024, **179**, 106492.

18 P. T. Williams and R. Bagri, *Int. J. Energy Res.*, 2004, **28**, 31–44.

19 M. Marczewski, E. Kaminska, H. Marczewska, M. Godek, G. Rokicki and J. Sokolowski, *Appl. Catal., B*, 2013, **129**, 236–246.

20 G. C. Hwang, J. H. Choi, S. Y. Bae and H. Kumazawa, *Korean J. Chem. Eng.*, 2001, **18**, 854–861.

21 S. K. Choi, Y. S. Choi, Y. W. Jeong, S. Y. Han and Q. V. Nguyen, *Biomass Bioenergy*, 2023, **177**, 106933.

22 M. Artetxe, G. Lopez, M. Amutio, I. Barbarias, A. Arregi, R. Aguado, J. Bilbao and M. Olazar, *Waste Manage.*, 2015, **45**, 126–133.

23 Y. R. Liu, J. L. Qian and J. Q. Wang, *Fuel Process. Technol.*, 2000, **63**, 45–55.

24 T. Faravelli, M. Pinciroli, F. Pisano, G. Bozzano, M. Dente and E. Ranzi, *J. Anal. Appl. Pyrolysis*, 2001, **60**, 103–121.

25 P. T. Williams and E. A. Williams, *Environ. Technol.*, 1999, **20**, 1109–1118.

26 R. Aguado, M. Olazar, B. Gaisán, R. Prieto and J. Bilbao, *Chem. Eng. J.*, 2003, **92**, 91–99.

27 S. S. Kim and S. Kim, *Chem. Eng. J.*, 2004, **98**, 53–60.

28 D. S. Achilias, I. Kanellopoulou, P. Megalokonomos, E. Antonakou and A. A. Lappas, *Macromol. Mater. Eng.*, 2007, **292**, 923–934.

29 M. W. Lodewyk, M. R. Siebert and D. J. Tantillo, *Chem. Rev.*, 2012, **112**, 1839–1862.

30 T. Lu, *J. Chem. Phys.*, 2024, **161**, 082503.

31 T. M. Kruse, O. S. Woo, H.-W. Wong, S. S. Khan and L. J. Broadbelt, *Macromolecules*, 2002, **35**, 7830–7844.

32 T. M. Kruse, H. W. Wong and L. J. Broadbelt, *Ind. Eng. Chem. Res.*, 2003, **42**, 2722–2735.